SPINE Volume 33, Number 1, pp 27–32

In Vivo Assessment of Lumbar Vertebral Strength in Elderly Women Using Computed Tomography-Based Nonlinear Finite Element Model

Kazuhiro Imai, MD, PhD,*† Isao Ohnishi, MD, PhD,* Seizo Yamamoto, MD, PhD,† and Kozo Nakamura, MD, PhD*

Study Design. *In vivo* study of a computed tomography (CT)-based nonlinear finite element model (FEM).

Objective. To establish an FEM with the optimum element size to assess the vertebral strength by comparing analyzed data with those obtained from mechanical testing *in vitro*, and then to assess the second lumbar (L2) vertebral strength *in vivo*.

Summary of Background Data. FEM has been reported to predict vertebral strength *in vitro*, but has not been used clinically.

Methods. Comparison among the 3 models with a different element size of 1 mm, 2 mm, and 3 mm was performed to determine which model achieved the most accurate prediction. Vertebral strength was assessed in 78 elderly Japanese women using an FEM with the optimum element size.

Results. The optimum element size was 2 mm. The L2 vertebral strength obtained with the FEM was 2154 ± 685 N, and the model could detect preexisting vertebral fracture better than measurement of bone mineral density.

Conclusion. The FEM could assess vertebral strength *in vivo*.

Key words: vertebral strength, osteoporosis, finite element model, elderly women, *in vivo* assessment. **Spine 2008;33:27–32**

Osteoporotic vertebral fractures have become a major social problem because the elderly population continues to increase. Vertebral fractures affect approximately 25% of postmenopausal women.[1] Measurement of the bone mineral density (BMD) by quantitative computed tomography (QCT) and dual energy radiograph absorptiometry (DXA) have been used to predict the risk of vertebral fracture. However, the correlation between vertebral bone strength and BMD measured by QCT is reported to be only 0.37 to 0.74,[2–7] while the correlation achieved with DXA is reported to be 0.51 to 0.80.[5–9] Therefore, such methods only explain 37% to 80% of vertebral strength. Bone strength primarily reflects the bone density and bone quality, which are influenced by bone architecture, turnover, accumulation of damage, and mineralization.[10]

It has been reported that a CT-based nonlinear finite element model (FEM) could predict vertebral strength and fracture sites accurately *in vitro*.[11] To predict quantitative strength and fracture sites is essential for the clinical application of an FEM because both parameters are important indicators of vertebral fracture risk. Prediction by an FEM with a smaller element size using the data from computed tomography (CT) scans with a thinner slice thickness and a smaller pixel size is thought to be more accurate. On the other hand, thinner CT slices lead to more radiation exposure in the clinical situation. To decrease radiation exposure as much as possible during CT scanning, optimization of the element size of the FEM was performed by assessing the accuracy of the FEM simulation.

The purposes of this study were to establish a CT-based nonlinear FEM with the optimum element size to predict the vertebral fracture load by evaluating the accuracy of our model from a comparison between predictions and data obtained by mechanical testing of human cadaver specimens *in vitro*, and then to assess lumbar vertebral strength in elderly women using the optimized CT-based nonlinear FEM.

■ Materials and Methods

Optimization of the Element Size of the FEM. This study used CT data and mechanical testing data obtained previously.[11] Twelve thoracolumbar vertebrae (T11, T12, and L1) with no skeletal pathology were collected within 24 hours of death from 4 men (31, 55, 67, and 83 years old). The vertebrae were disarticulated, and the discs were excised. Then the posterior element of each vertebra was removed by cutting through the pedicles. The vertebrae were immersed in water and axial CT scans with a slice thickness of 1 mm and a pixel width of 0.351 mm were obtained using a Lemage SX/E (GE Yokokawa Medical System, Tokyo, Japan) with a calibration phantom containing hydroxyapatite rods.

The 3-dimensional FEM was constructed from CT data using Mechanical Finder software (Mitsubishi Space Software Co., Tokyo, Japan). Three models with a different element size were created for each vertebra using 1 mm, 2 mm, or 3 mm tetrahedral elements. To the outer surface of the tetrahedral elements, triangular plates were attached as to form a cortical

From the *Department of Orthopaedic Surgery, School of Medicine, Tokyo University, Bunkyo-ku, Tokyo, Japan; and †Department of Orthopaedic Surgery, Tokyo Metropolitan Geriatric Medical Center, Itabashi-ku, Tokyo, Japan.

This work has been supported by the grant in aid for Scientific Research received from Japan Society for the Promotion of Science.

Acknowledgment date: March 27, 2007. Revision date: June 8, 2007. Acceptance date: July 2, 2007.

The manuscript submitted does not contain information about medical device(s)/drug(s).

No funds were received in support of this work. No benefits in any form have been or will be received from a commercial party related directly or indirectly to the subject of this manuscript.

Address correspondence and reprint requests to Isao Ohnishi, MD, PhD, Department of Orthopaedic Surgery, School of Medicine, Tokyo University, 7-3-1 Hongo, Bunkyo-ku, Tokyo 113-0033, Japan; E-mail: ohnishi-i@umin.ac.jp

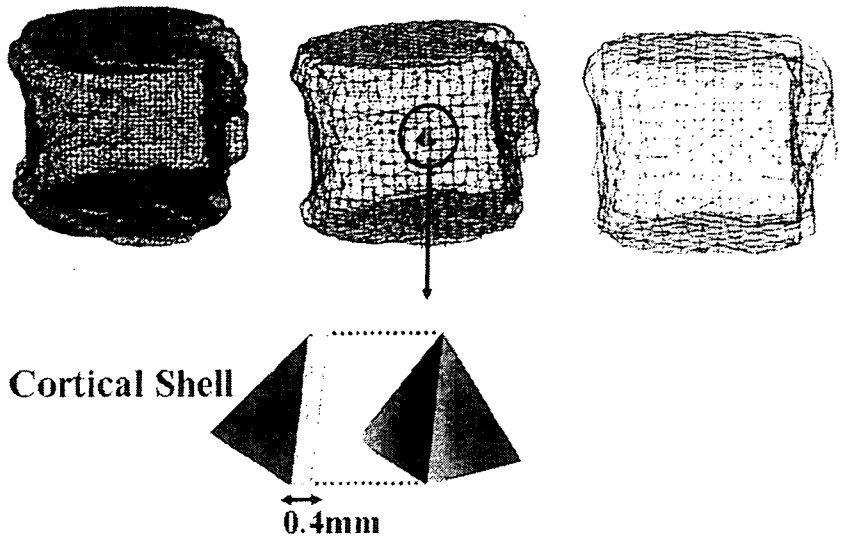

Figure 1. Finite element models of a whole vertebral body constructed with 1 mm, 2 mm, or 3 mm tetrahedral elements. The cortical shell was modeled by using triangular plates with a thickness of 0.4 mm. The model on the left consists of 104,205 nodes with 585,784 tetrahedral elements and 15,800 triangular plates constructed using 1-mm size elements. The middle model consists of 12,938 nodes with 70,022 tetrahedral elements and 3586 triangular plates constructed using 2-mm elements. The model on the right consists of 3476 nodes with 18,103 tetrahedral elements and 1330 triangular plates constructed using 3-mm size elements.

shell (Figure 1). The thickness of this shell was set as 0.4 mm based on the previous papers.[12–14]

To allow for bone heterogeneity, the mechanical properties of each element were computed from the Hounsfield unit value. Ash density of each voxel was determined from the linear regression equation created by these values of the calibration phantom. Ash density of each element was set as the average ash density of the voxels contained in one element. Young's modulus and the yield stress of each tetrahedral element were calculated from the equations proposed by Keyak *et al.*[15] Young's modulus of each triangular plate was set as 10 GPa and Poisson's ratio of each element was set as 0.4.

A uniaxial compressive load with a uniform distribution was applied on the upper surface of the vertebra and all the elements and all the nodes of the lower surface were completely restrained. Each model was analyzed using Mechanical Finder software as reported previously.[11]

A nonlinear FEM by Newton-Raphson method was used. To allow for the nonlinear phase, mechanical properties of the elements were assumed to be bilinear elastoplastic, and the isotropic hardening modulus was set as 0.05. Each element was assumed to yield when its Drucker-Prager equivalent stress reached the element yield stress. In the postyield phase, failure was defined as occurring when the minimum principal strain of an element was less than −10,000 microstrain.

The predicted fracture load was defined as the load that caused at least one element failure, while the measured fracture load was defined as the ultimate load that was achieved by mechanical testing. Pearson's correlation analysis was used to evaluate correlations between the fracture load predicted by FEM simulation and the measured fracture load. To optimize the element size of the FEM, the accuracy of prediction of the fracture load was compared among the 3 models with different element sizes. To assess the relationship between the models with a different element size, linear regression analyses were performed.

In addition, we also created models using 1.4 mm and 4.5 mm elements as well as 1 mm, 2 mm, and 3 mm elements to investigate the model convergence. For each of the models, total strain energy was calculated at a load of 1000 N, under which all specimens were in the elastic phase. Data on the total strain energy were compared among the 1 mm (average 403,033 tetrahedral elements), 1.4 mm (average 143,367 tetrahedral elements), 2 mm (average 47,687 tetrahedral elements), 3 mm (average 11,903 tetrahedral elements), and 4.5 mm (average 2719 tetrahedral elements) models.

***In Vivo* Assessment of Lumbar Vertebral Strength.** The subjects were ambulatory postmenopausal Japanese women aged 60 to 85 years. Excluded from participation were women with disorders of bone and mineral metabolism other than postmenopausal osteoporosis, those who had any recent or current treatment with the potential to alter bone turnover or bone metabolism, and those with a history of second lumbar vertebral (L2) fracture. The study protocol was approved by our ethics committee and each participant provided written informed consent. A total of 78 eligible participants were enrolled in this study.

In all the participants, the BMD (g/cm^2) of the lumbar spine (L2–L4) was measured by DXA (DPX; Lunar, Madison, WI) in the supine position and axial CT scans of L2 were obtained with a slice thickness of 2 mm and pixel width of 0.35 mm using Light Speed QX/i (GE Yokokawa Medical System, Tokyo, Japan) with a calibration phantom containing hydroxyapatite rods. The 3-dimensional FEM was constructed from the CT data using Mechanical Finder with 2 mm tetrahedral elements and 2 mm triangular plates, and the fracture load was analyzed using this software as described above.

Results are expressed as the mean ± standard deviation (SD). Statistical analysis was performed with the Mann-Whitney *U* test and the Kruskal-Wallis test. Differences were considered significant at $P < 0.05$.

■ Results

Optimization of the FEM Element Size

There was a strong linear correlation between the fracture load predicted by the FEM with 1 mm tetrahedral elements and the measured loads ($r = 0.938$, $P < 0.0001$), and the slope of the regression line was 0.934 (Figure 2A). With 2 mm elements, the correlation was even stronger ($r = 0.978$, $P < 0.0001$), and the slope of the regression line was 0.881 (Figure 2B). With 3 mm elements, the correlation was slightly weaker ($r = 0.866$, $P < 0.0001$), and the slope of the regression line was

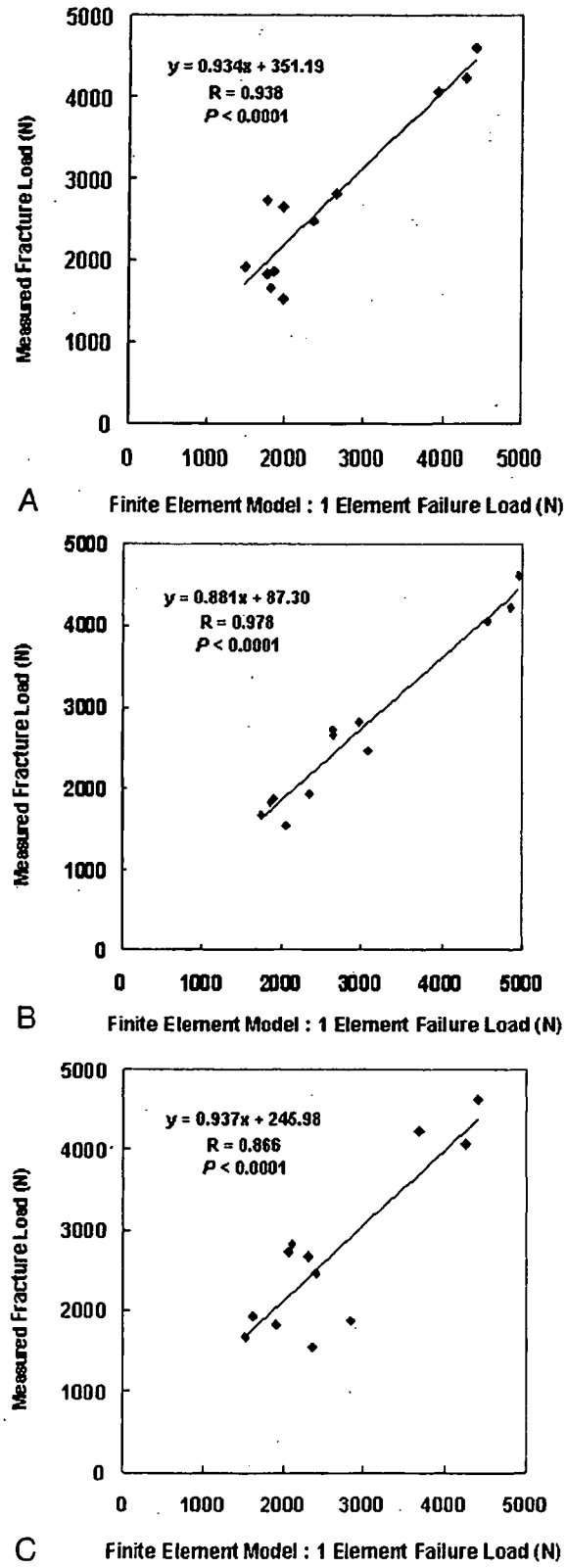

Figure 2. The measured fracture load *versus* the fracture load predicted by the finite element model (FEM). **A**, FEM with-1 mm tetrahedral elements. **B**, FEM with-2 mm tetrahedral elements. **C**, FEM with 3-mm tetrahedral elements. Strong correlations ($r > 0.90$) were obtained with elements of 1 mm and 2 mm in size, while a moderate correlation ($r = 0.866$) was obtained with 3-mm elements.

0.937 (Figure 2C). There was a strong linear correlation between the fracture load predicted by the 1 mm element model and that by the 2 mm ($r = 0.959$, $P < 0.0001$), and the slope of the regression line was 0.868. With the 1 mm and 3 mm models, the correlation was slightly weaker ($r = 0.912$, $P < 0.0001$), and the slope of the regression line was 0.839. With the 2 mm and 3 mm models, the correlation was much weaker ($r = 0.878$, $P < 0.0001$), and the slope of the regression line was 0.730.

In the convergence study, total strain energy decreased by 9.1% (4.0%–22.9%), with an increase of the element size from 1 mm to 1.4 mm. With an increase from 1.4 mm to 2 mm, it decreased by 10.0% (6.5%–17.3%), and decreased by 9.5% (2.9%–13.2%) from 2 mm to 3 mm. With an increase from 3 mm to 4.5 mm, total strain energy increased in some vertebrae although it decreased by an average of 38.6%.

In Vivo *Assessment of Lumbar Vertebral Strength*

The 78 women enrolled in the study had a mean age of 74.4 ± 5.6 years, a mean height of 148.4 ± 6.0 cm, and a mean weight of 50.3 ± 7.7 kg. The measured BMD of the lumbar spine was 0.808 ± 0.181 g/cm^2 and the strength of L2 predicted by the model was 2154 ± 685 N.

The subjects were classified into 5-year age groups, as summarized in Table 1. Height and vertebral strength showed a significant decrease in the older age groups, but weight and BMD did not change significantly (Kruskal-Wallis test, $P < 0.05$).

Next, the subjects were classified on the basis of prior vertebral fracture. Among the 78 women, 42 did not have any vertebral fractures (nonfracture group) and 36 subjects already had vertebral fractures (fracture group). Thus, vertebral fractures were present in 46.1% of the total study population. The characteristics of the 2 groups are summarized in Table 2. The nonfracture group was significantly younger than the fracture group (Mann-Whitney *U* test, $P < 0.001$). Height ($P < 0.05$) and weight ($P < 0.005$) were significantly greater in the nonfracture group than in the fracture group.

The average spinal BMD of the nonfracture group was 0.849 ± 0.146 g/cm^2, which was greater than that of the fracture group at 0.759 ± 0.207 g/cm^2 ($P < 0.05$) (Figure 3). The predicted vertebral strength of L2 was 2489 ± 580 N in the nonfracture group, which was greater than in the fracture group at 1764 ± 588 N ($P < 0.0001$) (Figure 3). The L2 strength to weight ratio was 4.80 ± 1.20 in the nonfracture group, and this was significantly greater than in the fracture group at 3.77 ± 1.36 ($P < 0.005$) (Figure 4).

■ Discussion

Assessing vertebral strength by using the FEM has been difficult because of the complex geometry, elastoplasticity, and thin cortical shell of the vertebra. The vertebrae have an elaborate architecture and geometry with curved surfaces, which cannot be modeled properly by using

Table 1. Summary of the Subjects' Height, Weight, BMD, and Analyzed Vertebral Strength (Mean ± SD)

Age (yr)	N	Height (cm)	Weight (kg)	BMD (g/cm^2)	Vertebral Strength (N)
60–64	6	153.5 ± 4.5	54.0 ± 6.1	0.850 ± 0.180	2592 ± 497
65–69	10	152.3 ± 7.8	50.9 ± 8.2	0.848 ± 0.112	2665 ± 528
70–74	21	148.1 ± 5.0	51.3 ± 7.4	0.744 ± 0.169	2050 ± 752
75–79	26	147.8 ± 6.2	48.5 ± 8.7	0.800 ± 0.200	2069 ± 706
80–85	15	145.1 ± 3.8	50.3 ± 6.3	0.867 ± 0.191	1933 ± 512

8-noded hexahedral elements. Previous mechanical tests have shown that there is a difference between the tensile and compressive strength of bone,[16–18] with compressive strength showing nonlinear behavior. Therefore, a nonlinear FEM should be used to predict the clinical fracture load. The cortical shell of each vertebra is estimated to have a thickness of approximately 0.4 mm.[12–14] In comparison, the resolution of clinically available CT scanners is fairly low, with a pixel spacing of larger than 0.25 mm. This means that the currently available CT data do not allow the thin cortical shell to be precisely modeled. The cortical thickness tends to be overestimated and its density is underestimated.[19,20] Therefore, it is necessary to construct a thinner model cortical shell from non-CT data. Shell elements of triangular plates with a uniform thickness of 0.4 mm were used to construct a cortical shell.

The characteristics of the present FEM in this study were as follows: adoption of the tetrahedral elements to model the surface curvature of the entire vertebra, utilization of nonlinear analysis to match the elastoplasticity of the vertebra during compression, and construction of a cortical shell as the surface of the model. It has been reported that the thin cortex of a vertebra contributes 12%–75% to its overall strength and the contribution of the cortex is estimated to be significantly larger in osteoporotic individuals.[21,22] Thus, the importance of the strength of the cortical shell should be taken into consideration when predicting the fracture load for osteoporosis patients.

The limitation of our model is that the cortical shell was treated as a homogenous material because the pixels of CT scans were too large to model the thin cortex. In addition, with the limited resolution of currently available CT scanners, the microarchitecture of the bone cannot be precisely assessed. Micro-CT and synchrotron micro-CT can visualize bone microstructure.[23] Therefore, an FEM based on micro-CT data may show more accurate simulation because it would be possible to model a cortical shell with heterogeneous properties and also to assess the microarchitecture. However, obtaining micro-CT scans of a whole vertebra *in vivo* would be impossible with the currently available scanners. Also, use of thinner CT slices to obtain images leads to more radiation exposure. To decrease radiation exposure for clinical use, somewhat thicker slices would be more appropriate.

Table 2. Background of the Subjects in No Fracture Group and Fracture Group

Group	N	Age (yr)	Height (cm)	Weight (kg)
No fracture group	42	72.3 ± 5.7	149.9 ± 5.7	52.6 ± 7.4
Fracture group	36	76.8 ± 4.6	146.6 ± 6.0	47.8 ± 7.3

We assessed 3 models each with a different element size of 1 mm, 2 mm, and 3 mm. With an element size of 1 mm and 2 mm, the correlation between the fracture load predicted by the FEM and that measured experimentally was very strong ($r > 0.90$). With an element size of 3 mm, the correlation was slightly weaker ($r < 0.90$). Although all of 3 FEM were generated using CT data obtained with a 1 mm slice thickness, these results suggested that the elements with a size of 1 mm or 2 mm could be used to accurately predict the fracture load. There was a stronger correlation ($r = 0.978$) with 2 mm tetrahedral elements than with either 1 mm or 3 mm elements. The correlation of the fracture load between the prediction and the experiment was better than that in the previous FEM studies ($r = 0.89–0.95$).[24–27] The slope of the regression line obtained with 2 mm tetrahedral elements was 0.881, which was also better than that in the previous FEM studies (0.569–0.86).[24–27] The previous FEM studies had failed to model the surface curvature of the vertebra, match the elastoplasticity of the vertebra, or model a cortical shell. These results indicated that our FEM predicted compressive vertebral strength more accurately.

The correlation between the fracture load with 1 mm and 2 mm elements ($r = 0.959$) was stronger than both of the correlations between 1 mm and 3 mm ($r = 0.912$), and between 2 mm and 3 mm ($r = 0.878$). The slope of the regression line relating 1 mm and 2 mm (0.868) was also better than that relating 1 mm and 3 mm (0.839), and that relating 2 mm and 3 mm (0.730). These results indicated that the prediction by the FEM with the 1 mm and 2 mm elements achieved more accurate result than the 3 mm elements.

The results obtained by the convergence study with the 1 mm, 1.4 mm, 2 mm, 3 mm, and 4.5 mm models suggested the model with 1 mm elements was the most accurate among the 5 models. However, the 2 mm model was thought to achieve sufficiently accurate prediction compared with the 1 mm model. In the previous FEM study using the models with 8-noded hexahedral elements, stiffness of the model with $3 \times 3 \times 3$ mm^3 elements was on average only 4% greater than that with

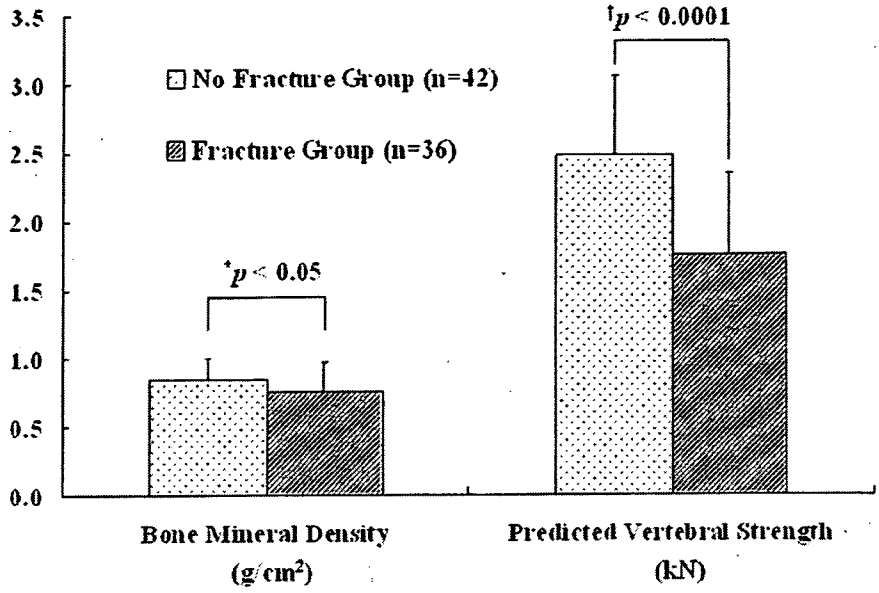

Figure 3. Bone mineral density of the lumbar spine (L2–L4) and predicted vertebral strength of the L2 vertebra in the nonfracture group (n = 42) and in the fracture group (n = 36). The error bars represent one standard deviation from the mean. Bone mineral density of the nonfracture group was greater than that of the fracture group. The difference was significant ($P < 0.05$). Predicted vertebral strength in the nonfracture group was also significantly ($P < 0.0001$) greater than that of the fracture group.

$1 \times 1 \times 1.5$ mm^3 elements, and there was a high correlation between the stiffness and the experimentally measured ultimate strength values in both $3 \times 3 \times 3$ mm^3 element model ($r^2 = 0.94$) and $1 \times 1 \times 1.5$ mm^3 element model ($r^2 = 0.92$).[28]

Based on these *in vitro* data, an *in vivo* study was performed using CT scans with a 2-mm slice thickness and a nonlinear FEM with an element size of 2 mm. There have been few reports about predicting vertebral strength *in vivo*, although some authors have assessed vertebral strength *in vitro* by mechanical testing. In the elderly, McBroom *et al* reported that among 10 specimens from subjects with an average age of 78 years, the average failure load for the L1 vertebral body was 3160 ± 424 N and it was 3385 ± 485 N for L3.[3] Eckstein *et al* reported that the average failure load for L3 was 3016 ± 149 N when they tested 102 specimens from the subjects with an average age of 80.6 years.[29] These 2 reports included both men and women. In the present study, however, all of the subjects were Japanese women. This might be one of the reasons why our predicted vertebral strength was smaller than that reported elsewhere.

The limitation in our study was that the prediction was made under a uniaxial compressive loading condition. In an *in vivo* situation, the loading and boundary conditions are completely different. However, one of the advantages of FEM simulation is that it allows us to set an arbitrary load magnitude or direction to simulate loading in various activities of daily living. If predicted strength by FEM was proved to be accurate in a uniaxial compressive loading condition, we could assume that we might be able to apply this method to predict accurately the strength under various other loading and boundary conditions. Nevertheless, the accuracy of our method in predicting strength under different loading and boundary conditions should be validated by conducting another mechanical testing and it would be one of our assignments in the future study.

In this study, the vertebral strength predicted by FEM could detect preexisting vertebral fractures better than

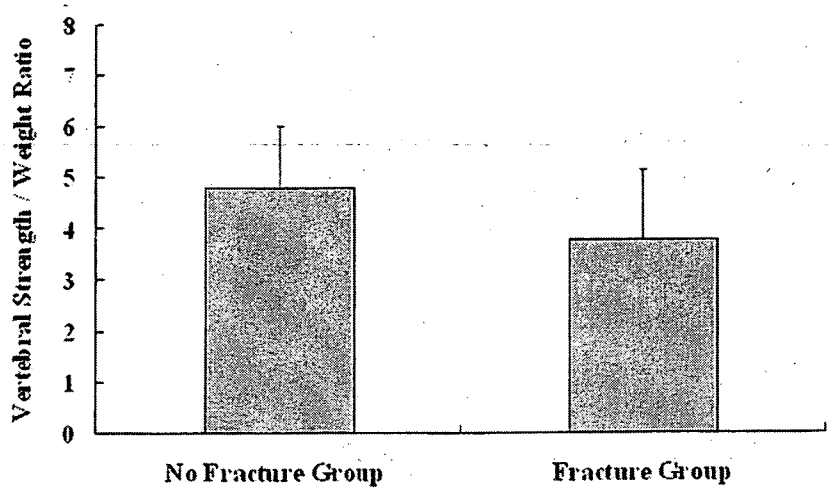

Figure 4. The ratio of L2 vertebral strength to weight in the nonfracture group (n = 42) and in the fracture group (n = 36). The difference was also significant ($P < 0.005$).

BMD. CT-based FEM assesses bone geometry and heterogeneous bone mass distribution as well as the BMD. It is hoped that CT-based FEM will become useful for estimating the risk of vertebral fracture in osteoporotic individuals.

■ Key Points

- *In vivo* assessment of lumbar vertebral strength in elderly Japanese women was performed using a CT-based nonlinear finite element model that was established and initially evaluated *in vitro*.
- The average L2 vertebral strength of the 78 subjects was 2154 ± 685 N according to this model.
- The present FEM could detect preexisting vertebral fracture more accurately than measurement of the bone mineral density.

References

1. Melton LJ. Epidemiology of spinal osteoporosis. *Spine* 1997;22(suppl):2–11.
2. Mosekilde L, Bentzen SM, Ortoft G, et al. The predictive value of quantitative computed tomography for vertebral body compressive strength and ash density. *Bone* 1989;10:465–70.
3. McBroom RJ, Hayes WC, Edwards WT, et al. Prediction of vertebral body compressive fracture using quantitative computed tomography. *J Bone Joint Surg Am* 1985;67:1206–14.
4. Brinckmann P, Biggemann M, Hilweg D, et al. Prediction of the compressive strength of human lumbar vertebrae. *Clin Biomech* 1989;4(suppl):1–27.
5. Edmondston SJ, Singer KP, Day RE, et al. In-vitro relationships between vertebral body density, size and compressive strength in the elderly thoracolumbar spine. *Clin Biomech* 1994;9:180–6.
6. Cheng XG, Nicholson PH, Boonen S, et al. Prediction of vertebral strength in vitro by spinal bone densitometry and calcaneal ultrasound. *J Bone Miner Res* 1997;12:721–8.
7. Eriksson SA, Isberg BO, Lindgren JU. Prediction of vertebral strength by dual photon absorptiometry and quantitative computed tomography. *Calcif Tissue Int* 1989;44:243–50.
8. Myers BS, Arbogast KB, Lobaugh B, et al. Improved assessment of lumbar vertebral body strength using supine lateral dual-energy x-ray absorptiometry. *J Bone Miner Res* 1994;9:687–93.
9. Biarnason K, Hassager C, Svendsen OL, et al. Anteroposterior and lateral spinal DXA for the assessment of vertebral body strength: comparison with hip and forearm measurement. *Osteoporosis Int* 1996;6:37–42.
10. NIH Consensus Development Panel on Osteoporosis Prevention D, and Therapy. Osteoporosis prevention, diagnosis, and therapy. *JAMA* 2001;285:785–95.
11. Imai K, Ohnishi I, Bessho M, et al. Nonlinear finite element model predicts vertebral bone strength and fracture site. *Spine* 2006;31:1789–94.
12. Silva MJ, Wang C, Keaveny TM, et al. Direct and computed tomography thickness measurements of the human, lumbar vertebral shell and endplate. *Bone* 1994;15:409–14.
13. Vesterby A, Mosekilde L, Gundersen HJ, et al. Biologically meaningful determinants of the in vitro strength of lumbar vertebrae. *Bone* 1991;12:219–24.
14. Mosekilde L. Vertebral structure and strength in vivo and in vitro. *Calcif Tissue Int* 1993;53(suppl):121–6.
15. Keyak JH, Rossi SA, Jones KA, et al. Prediction of femoral fracture load using automated finite element modeling. *J Biomech* 1998;31:125–33.
16. Keaveny TM, Wachtel EF, Ford CM, et al. Differences between the tensile and compressive strengths of bovine tibial trabecular bone depend on modulus. *J Biomech* 1994;27:1137–46.
17. Kopperdahl DL, Keaveny TM. Yield strain behavior of trabecular bone. *J Biomech* 1998;31:601–8.
18. Morgan EF, Keaveny TM. Dependence of yield strain of human trabecular bone on anatomic site. *J Biomech* 2001;34:569–77.
19. Dougherty G, Newman D. Measurement of thickness and density of thin structures by computed tomography: a simulation study. *Med Phys* 1999;26:1341–8.
20. Prevrhal S, Engelke K, Kalender WA. Accuracy limits for the determination of cortical width and density: the influence of object size and CT imaging parameters. *Phys Med Biol* 1999;44:751–64.
21. Faulkner KG, Cann CE, Hasegawa BH. Effect of bone distribution on vertebral strength: assessment with patient-specific nonlinear finite element analysis. *Radiology* 1991;179:669–74.
22. Rockoff SD, Sweet E, Bleustein J. The relative contribution of trabecular and cortical bone to the strength of human lumbar vertebrae. *Calcif Tissue Res* 1969;3:163–75.
23. Ito M. Assessment of bone quality using micro-computed tomography (micro-CT) and synchrotron micro-CT. *J Bone Miner Metab* 2005;23(suppl):115–21.
24. Silva MJ, Keaveny TM, Hayes WC. Computed tomography-based finite element analysis predicts failure loads and fracture patterns for vertebral sections. *J Orthop Res* 1998;16:300–8.
25. Martin H, Werner J, Andresen R, et al. Noninvasive assessment of stiffness and failure load of human vertebrae from CT-data. *Biomed Tech* 1998;43:82–8.
26. Liebschner MA, Kopperdahl DL, Rosenberg WS, et al. Finite element modeling of the human thoracolumbar spine. *Spine* 2003;28:559–65.
27. Crawford RP, Cann CE, Keaveny TM. Finite element models predict in vitro vertebral body compressive strength better than quantitative computed tomography. *Bone* 2003;33:744–50.
28. Crawford RP, Rosenberg WS, Keaveny TM. Quantitative computed tomography-based finite element models of the human lumbar vertebral body: effect of element size on stiffness, damage, and fracture strength predictions. *J Biomech Eng* 2003;125:434–8.
29. Eckstein F, Lochmüller EM, Lill CA, et al. Bone strength at clinically relevant sites displays substantial heterogeneity and is best predicted from site-specific bone densitometry. *J Bone Miner Res* 2002;17:162–71.

Prediction of strength and fracture location of the proximal femur by a CT-based nonlinear finite element method - Effect of load direction on hip fracture load and fracture site -

Masahiko Bessho, Isao Ohnishi, Takuya Matsumoto, Satoru Ohashi, Kenji Tobita, Juntaro Matsuyama, Kozo Nakamura
Orthopaedic Surgery, University of Tokyo, Tokyo, Japan
ohnishii-dis@h.u-tokyo.ac.jp

Introduction: The occurrence rate of hip fractures due to osteoporosis is rapidly increasing, representing one of the most serious and urgent social problems. We focused on a computed tomography-based finite element method (CT/FEM) to quantify structural strength, thereby developing a nonlinear CT/FEM to achieve accurate assessment of strength of the proximal femur [1]. The aim of this study was to investigate the effect of load direction on fracture risk of the proximal femur. For this purpose, we evaluated changes in magnitude of strength for the proximal femur with changes in load direction by analyzing the contralateral femur in patients with hip fracture using the nonlinear CT/FEM. We also verified changes in fracture risk by site. From these analyses, we identified load and boundary conditions that could increase risk of hip fracture and clarified that this could possibly cause the fracture types commonly seen in clinical situations.

Materials and Methods: Twenty eight femora in female patients with contralateral hip fracture (age: 80 - 91, average: 85.2)(femoral neck fracture: 13 patients, trochanteric fracture: 15 patients). The study protocol was approved by our ethics committee and the patients were enrolled after informed consent was given. Within 7 days after admission, axial CT images of the proximal femur were obtained (slice thickness: 3 mm, Aquilion Super 4, Toshiba Medical Systems Co., Tokyo, Japan) as well as scans of a calibration phantom. The CT data were transferred to a workstation and 3D finite element models were constructed from the CT data using Mechanical Finder (Research Center of Computational Mechanics Inc., Tokyo, Japan). Trabecular bone and the inner portion of cortical bone were modeled using 3 mm linear tetrahedral elements, while the outer cortex was modeled using 3 mm triangular plates (0.4 mm thick)[1]. On average, there were 75,212 tetrahedral elements and 4,103 triangular plates.

Force was applied to the femoral head at an angle γ to the shaft in the frontal plane and at an angle δ to the neck axis in the transverse plane (Fig. 1). For stance configuration (SC), γ and δ were set at 160° and 0°. For fall configuration (FC), γ and δ were set at 120° and 0° (FC1), 60° and 0° (FC2), 60° and 15° (FC3) or 60° and 45° (FC4), respectively [4, 5].

Materially nonlinear finite element analysis was performed by the Newton-Raphson method. Fracture was defined as occurring when at least one shell element failed. Fracture loads were predicted and sites at fracture risk were identified [1].

Correlations between predicted fracture load and load direction were investigated. Predicted fracture type was compared with contralateral actual fracture type.

Pearson's correlation analysis, Friedman test, Scheffe's post hoc test and Fisher's exact test were used for statistical analyses and the results were considered significant when p values were less than 0.05.

Results: The average predicted fracture loads for SC was 3080 N (standard deviation (SD): 551 N), 2210 N (SD: 606 N) for FC1, 1047 N (SD: 236 N) for FC2, 970 N (SD: 199 N) for FC3 and 700 N (SD: 167 N) for FC4, respectively.

The predicted fracture loads for SC were significantly higher than those for all fall configurations except for FC1 ($p < 0.001$).

In comparisons of predicted fracture loads for all fall configurations, loads were significantly higher for FC1 than for FC2, FC3 or FC4 ($p=0.02$, $p<0.001$, $p<0.001$, respectively).

The predicted fracture loads for FC2 were significantly higher than those for FC4 ($p < 0.001$). The predicted fracture loads for FC3 were significantly higher than those for FC4 ($p < 0.01$).The correlations of the predicted fracture loads for all configurations were shown on Table 1.

The predicted fracture sites located at sub-capital region in all patients for SC. The predicted sites located at trochanteric region in all patients for all fall loading configurations except for FC1. For FC1, the predicted sites located at sub-capital region in13 patients, but in 15 patients, they located at trochanteric region. For 20 patients, contralateral actual fracture type corresponded to predicted fracture type. Predicted fracture type corresponded significantly to contralateral actual fracture type ($p<0.01$).

Discussion: As δ increases, the fall tends to be directed more posteriorly. Falls in a posterolateral direction were thus indicated to increase fracture risk more than falls to the side. Each of the predicted fracture loads from various loading conditions displayed poor correlation with each other, even though most correlations were significant. Strength of the proximal femur should thus be evaluated under multiple loading conditions. Intertrochanteric fractures were predicted to occur under all fall loading conditions except FC1. Hirsch et al. reported that compressive force along the long axis of the femoral neck is necessary for femoral neck fractures to occur [6]. Mean neck-shaft angle of the femur is known to be 120°-130°, so FC1 was considered as the condition that could cause neck fractures. If we assume that no morphological differences exist between right and left femora in each patient [7], in all fall loading conditions except FC1, the loading condition would possibly be the only decisive factor for fracture type, irrespective of the morphological characteristics of each patient. Conversely, in FC1, fracture type might differ depending on morphological characteristics of each patient. Keyak et al. reported relationships between loading direction and magnitude of predicted fracture load [4]. However, they reported results from only 4 patients and statistical analyses were not conducted. In addition, they lacked information on predicted fracture sites. The present study could contribute to providing us with useful information for the establishment of effective measures to prevent hip fractures.

References: [1] Bessho et al. J Biomech 40: 1745-53, 2007 [2] Keyak et al., J Biomed Mater Res 28: 1329-36, 1994 [3] Keller et al., J Biomech 27: 1159-68, 1994 [4] Keyak et al., J Orthop Res 19: 539-44, 2001 [5] Fujii et al., Nippon Seikeigeka Gakkai Zasshi 61: 531-41, 1987 [6] Hirsch et al., J Bone Joint Surg Br 42: 633-40, 1960 [7] Boston et al., Injury 14: 207-10, 1982

Table 1. Correlations (r) of the predicted fracture loads for each loading configurations.

	SC	FC1	FC2	FC3	FC4
SC	-	n.s.	0.52	0.55	0.67
FC1	n.s.	-	0.55	0.55	0.49
FC2	0.52	0.55	-	0.88	0.67
FC3	0.55	0.55	0.88	-	0.81
FC4	0.67	0.49	0.67	0.81	-

n.s.: not significant

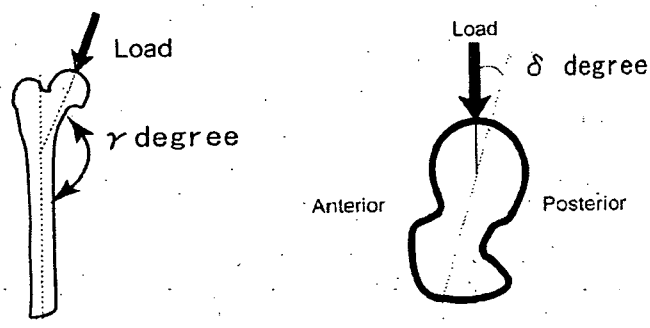

Fig. 1. Force direction

Prediction of strength and fracture location of the proximal femur by a CT-based nonlinear finite element method - Effect of load direction on hip fracture load and fracture site -

Masahiko Bessho, Isao Ohnishi, Takuya Matsumoto, Satoru Ohashi, Kenji Tobita, Juntaro Matsuyama, Kozo Nakamura
Orthopaedic Surgery, University of Tokyo, Tokyo, Japan
ohnishii-dis@h.u-tokyo.ac.jp

Introduction: The occurrence rate of hip fractures due to osteoporosis is rapidly increasing, representing one of the most serious and urgent social problems. We focused on a computed tomography-based finite element method (CT/FEM) to quantify structural strength, thereby developing a nonlinear CT/FEM to achieve accurate assessment of strength of the proximal femur [1]. The aim of this study was to investigate the effect of load direction on fracture risk of the proximal femur. For this purpose, we evaluated changes in magnitude of strength for the proximal femur with changes in load direction by analyzing the contralateral femur in patients with hip fracture using the nonlinear CT/FEM. We also verified changes in fracture risk by site. From these analyses, we identified load and boundary conditions that could increase risk of hip fracture and clarified that this could possibly cause the fracture types commonly seen in clinical situations.

Materials and Methods: Twenty eight femora in female patients with contralateral hip fracture (age: 80 - 91, average: 85.2)(femoral neck fracture: 13 patients, trochanteric fracture: 15 patients). The study protocol was approved by our ethics committee and the patients were enrolled after informed consent was given. Within 7 days after admission, axial CT images of the proximal femur were obtained (slice thickness: 3 mm, Aquilion Super 4, Toshiba Medical Systems Co., Tokyo, Japan) as well as scans of a calibration phantom. The CT data were transferred to a workstation and 3D finite element models were constructed from the CT data using Mechanical Finder (Research Center of Computational Mechanics Inc., Tokyo, Japan). Trabecular bone and the inner portion of cortical bone were modeled using 3 mm linear tetrahedral elements, while the outer cortex was modeled using 3 mm triangular plates (0.4 mm thick)[1]. On average, there were 75,212 tetrahedral elements and 4,103 triangular plates.

Force was applied to the femoral head at an angle γ to the shaft in the frontal plane and at an angle δ to the neck axis in the transverse plane (Fig. 1). For stance configuration (SC), γ and δ were set at 160° and 0°. For fall configuration (FC), γ and δ were set at 120° and 0° (FC1), 60° and 0° (FC2), 60° and 15° (FC3) or 60° and 45° (FC4), respectively [4, 5].

Materially nonlinear finite element analysis was performed by the Newton-Raphson method. Fracture was defined as occurring when at least one shell element failed. Fracture loads were predicted and sites at fracture risk were identified [1].

Correlations between predicted fracture load and load direction were investigated. Predicted fracture type was compared with contralateral actual fracture type.

Pearson's correlation analysis, Friedman test, Scheffe's post hoc test and Fisher's exact test were used for statistical analyses and the results were considered significant when p values were less than 0.05.

Results: The average predicted fracture loads for SC was 3080 N (standard deviation (SD): 551 N), 2210 N (SD: 606 N) for FC1, 1047 N (SD: 236 N) for FC2, 970 N (SD: 199 N) for FC3 and 700 N (SD: 167 N) for FC4, respectively.

The predicted fracture loads for SC were significantly higher than those for all fall configurations except for FC1 ($p < 0.001$).

In comparisons of predicted fracture loads for all fall configurations, loads were significantly higher for FC1 than for FC2, FC3 or FC4 ($p=0.02$, $p<0.001$, $p<0.001$, respectively).

The predicted fracture loads for FC2 were significantly higher than those for FC4 ($p < 0.001$). The predicted fracture loads for FC3 were significantly higher than those for FC4 ($p < 0.01$).The correlations of the predicted fracture loads for all configurations were shown on Table 1.

The predicted fracture sites located at sub-capital region in all patients for SC. The predicted sites located at trochanteric region in all patients for all fall loading configurations except for FC1. For FC1, the predicted sites located at sub-capital region in13 patients, but in 15 patients, they located at trochanteric region. For 20 patients, contralateral actual fracture type corresponded to predicted fracture type. Predicted fracture type corresponded significantly to contralateral actual fracture type ($p<0.01$).

Discussion: As δ increases, the fall tends to be directed more posteriorly. Falls in a posterolateral direction were thus indicated to increase fracture risk more than falls to the side. Each of the predicted fracture loads from various loading conditions displayed poor correlation with each other, even though most correlations were significant. Strength of the proximal femur should thus be evaluated under multiple loading conditions. Intertrochanteric fractures were predicted to occur under all fall loading conditions except FC1. Hirsch et al. reported that compressive force along the long axis of the femoral neck is necessary for femoral neck fractures to occur [6]. Mean neck-shaft angle of the femur is known to be 120°-130°, so FC1 was considered as the condition that could cause neck fractures. If we assume that no morphological differences exist between right and left femora in each patient [7], in all fall loading conditions except FC1, the loading condition would possibly be the only decisive factor for fracture type, irrespective of the morphological characteristics of each patient. Conversely, in FC1, fracture type might differ depending on morphological characteristics of each patient. Keyak et al. reported relationships between loading direction and magnitude of predicted fracture load [4]. However, they reported results from only 4 patients and statistical analyses were not conducted. In addition, they lacked information on predicted fracture sites. The present study could contribute to providing us with useful information for the establishment of effective measures to prevent hip fractures.

References: [1] Bessho et al. J Biomech 40: 1745-53, 2007 [2] Keyak et al., J Biomed Mater Res 28: 1329-36, 1994 [3] Keller et al., J Biomech 27: 1159-68, 1994 [4] Keyak et al., J Orthop Res 19: 539-44, 2001 [5] Fujii et al., Nippon Seikeigeka Gakkai Zasshi 61: 531-41, 1987 [6] Hirsch et al., J Bone Joint Surg Br 42: 633-40, 1960 [7] Boston et al., Injury 14: 207-10, 1982

Table 1. Correlations (r) of the predicted fracture loads for each loading configurations.

	SC	FC1	FC2	FC3	FC4
SC	-	n.s.	0.52	0.55	0.67
FC1	n.s.	-	0.55	0.55	0.49
FC2	0.52	0.55	-	0.88	0.67
FC3	0.55	0.55	0.88	-	0.81
FC4	0.67	0.49	0.67	0.81	-

n.s.: not significant

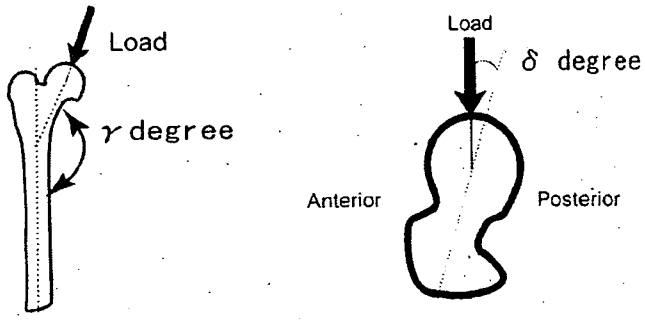

Fig. 1. Force direction

AN ASYMMETRICAL THREAD PROFILE EXTERNAL FIXATION PIN HAS HIGHER PULLOUT STRENGTH THAN A SYMMETRICAL THREAD PIN

Satoru Ohashi, Isao Ohnishi, Juntaro Matsuyama, Masahiko Bessho, Takuya Matsumoto, Kozo Nakamura
Department of Orthopaedic Surgery, Faculty of Medicine, University of Tokyo, Tokyo, Japan
soohashi-tky@umin.ac.jp

Introduction: One of the common complications in external fixation is pin loosening, which is suggested to be caused by stress concentration at the pin-bone interface [1, 4]. It could be minimized by utilizing improved thread profile design of the pins [4]. There have been several studies investigating the relationship between pin thread profile and pin pullout strength or pin-bone interface stress by conducting mechanical testing [2, 5] or by finite element (FE) method [3]. The thread configurations, however, in those studies were all symmetrical and no study has investigated mechanics of asymmetrical thread pins. We hypothesized mechanical performance of asymmetrical thread profile pins could be different from that of symmetrical pins. The purpose of this study was to investigate the mechanical performance of the asymmetrical pins by conducting pullout testing. Concurrently, three-dimensional FE models for the simulation of the pullout testing were created, thereby investigating the energy and stress distributions at the pin-bone interface using FE analysis.

Materials and Methods: Based on ISO 9268: 1988, we manufactured three different thread profile screw pins with an outer diameter of 6mm, an inner diameter of 4.8mm and a pitch of 1.8mm made of 6 Aluminum 4 Vanadium Titanium alloy. One had symmetrical thread and the other two were asymmetrically threaded. For the mechanical testing, 6mm thick epoxy-sheets (E-glass-filled Epoxy Sheet, 3001-04, Sawbones®, Pacific Research Laboratories, Inc., Vashon, WA) were used as cortical bone models. Pre-drilling the model using a 4.5 mm diameter drill bit was preceded before the pins were inserted with self-tapping technique. 6 pins were tested for each thread type. Pullout testing was conducted using a metal stopper with a 14 mm diameter round hole to restrain upward displacement of the bone model. Pins were pulled up with a mechanical testing machine (Servopulser EHF-LB5KN-10L, Shimazu, Kyoto, Japan) at a cross head speed of 0.03 mm/sec, based on the ASTM, F543-02 guidelines. The load was measured by a load cell (SCL-5KN, Shimazu, Kyoto, Japan) with a range of 7.5 kN. The pullout strength was defined as the ultimate strength achieved and described as a mean and a standard deviation (SD). The results of the mechanical tests were statistically analyzed by the analysis of variance. The differences were considered significant when p-values were less than 0.05.

Pullout testing simulation was performed using a FE method for the asymmetrical thread pins under a condition identical to the mechanical testing. Three-dimensional surface data in a computer assisted designing format for the screw pins and the cortical bone model were put into the mesh generation software (ANSYS ICEM CFD 5.1, Ansys Inc. Canonsburg, PA). FE mesh models of the pins and the bone model were created using tetrahedral elements with a variable side length of 0.5 to 1.0 mm by the oct-tree algorithm method. The average numbers of nodes and elements were 23,000 and 120,000, respectively. These meshes were imported into a finite element analysis software (Mechanical Finder software, RCCM, Tokyo, Japan). Young's moduli of the screws and the bone model were assumed to be isotropic, and assigned as that of 6 Aluminum 4 Vanadium Titanium (109.4 GPa) for the pins and that of the epoxy-sheet (12.4 GPa) used in the mechanical testing. Poisson's ratio was set as 0.28 for the pins and 0.4 for the bone model. A simulated uniaxial pullout load was applied at the end of the pin along its long axis. In order to simulate the contact interfacial characteristics between the screw pin and the bone model, node-on-node gap elements were created on the interface nodes. Virtual length of the gap elements was set as 0.1mm. Young's modulus of the gap element was set as the mean modulus of the pin and that of the bone model. The friction coefficient was set as 0.3. Linear analysis was performed with a pullout load of 4000 N. The average computing time was about 10 h. In post processing analysis, the pin-bone interface strain energy and stress concentration were assessed by analyzing the maximum strain energy density and the maximum equivalent stress (von Mises stress). The maximum strain energy density and the maximum equivalent stress were defined as the maximum values of the strain energy density and the equivalent stress of all bone elements.

Results: The measured pullout strength for the type A pin was significantly higher than that for the symmetrical thread pin and the type B pin ($p < 0.0001$). The maximum strain energy density and the maximum equivalent stress obtained from FE analysis for each pin were listed on Table 2. The maximum strain energy density and the maximum equivalent stress for the type A pin was the smallest of all pins. Each bone element with the maximum strain energy density or the maximum equivalent stress located at the pin-bone interface of each pin-bone complex model.

Discussion: From the results of the FE analysis, it was assumed the lower energy or stress concentration at the pin-bone interface of type A pin contributed to its significantly higher pullout strength in the mechanical testing. By adopting the asymmetrical thread pins, we may be able to enhance fixation by external fixators, thereby lowering the risk of pin loosening.

References: 1. Aro HT et al, J Trauma, 35, 1993; 2. Halsey D et al, Clin Orthop Relat Res, 278, 1992; 3. Hansson S et al, J Biomech, 36, 2003; 4. Huiskes R et al, J Orthop Res, 3, 1985; 5. Liu J et al, Clin Orthop Relat Res, 310, 1995

Acknowledgements: This work was funded by the grant in aid of the 15th Medical Frontier Project of Pharmaceuticals and Medical Devices Agency (PMDA) of Japan.

	Type A pin	Symmetrical pin	Type B pin
Pullout strength (N)	4668.3 ± 44.6	4333.3 ± 46.0	4281.3 ± 95.0
Maximum strain energy density (MJm3)	2.28	4.12	3.83
Maximum equivalent stress (MPa)	179.69	402.13	379.84

Values are described as the mean ± standard deviation.

The total angle of the thread tip was 45 degrees for all pins. The angle β and γ are defined as shown on the scheme and set as 22.5° and 22.5° for the symmetrical thread pin, 40.0° and 5.0° for type A pin, and 5.0° and 40.0° for type B pin, respectively.

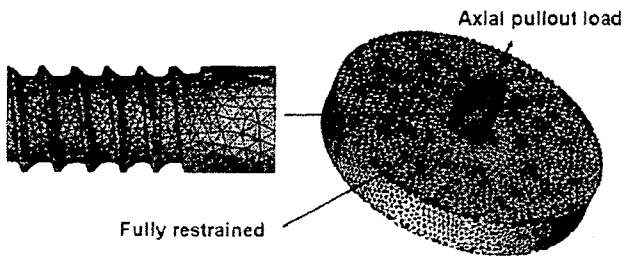

Each of the screw models was inserted in the center of a circular disk with a thickness of 6 mm and a diameter of 40mm, which simulated the cortical bone model.

75

3次元CT画像とCADデータを用いた手術シミュレーションの試み

Preoperative simulation using 3 dimensional CT and CAD datum

○松本 卓也、大西五三男、飛田 健治、大橋　暁、別所 雅彦、中村 耕三

東京大学医学部整形外科

長管骨変形治癒合に対して種々の創外固定器による変形矯正が幅広く行われている。矯正の為に創外固定器上にヒンジを設置、もしくはバーチャルヒンジを設定してレントゲンを基にした正面･側面の2次元変形角度の矯正を行う回旋変形の評価はCT画像を必要とする。2006年第19回本学会において大西らにより発表されたユニバーサル・バー・リンク機構を有する片側式創外固定器(UBL)を用いた変形矯正術前計画に際し、CTデータより3次元構築した患者固有の3次元骨モデルを用いた3次元変形矯正術前計画/手術シミュレーションを試みた。撮影したCT dicomデータを使用し、レキシー(株)のZed Viewを用い骨領域を抽出、患者固有の骨STLモデルを作成。同社との産学協同で開発したソフトを用い、作成した3Dモデルから設定したCORAを参照し、骨切面を設定。UBLのCADデータを用いて、手術手技どおりに近位部にピンを設置、UBLの各ヒンジの角度設定を行い遠位ピン刺入部の最適な設置部位を決定し、設置。設定完了することにより手術シミュレーションが完了する。骨切により分離した骨片は各ヒンジの角度を変化させることによりCORAを中心に動き、術前計画どおりに健側同様のベクトル角度をとるように移動する。STLモデルはコンピュータ画面上で自由に動かせるため多方面から変形を評価する事ができるため2Dのレントゲン写真だけでは評価が難しい回旋変形も容易に評価できる。本ソフトを臨床応用し、より高精度に変形矯正を行いたい。

3次元CT画像を基にした管骨変形評価法

Deformity Evaluation of the Tubular Bone Using 3D CT Image

東京大学医学部整形外科 ○飛田健治、大西五三男、別所雅彦、松本卓也
大橋暁、中村耕三

背景：長管骨の変形手術の術前計画は精確性を要する。Paleyら(1992)による術前計画法は正面･側面の単純レントゲン写真から変形量、変形中心(CORA)を求める方法を確立したが、レントゲンのみでは精確な術前計画は難しく、再現性を欠く。村瀬ら(2006, 2007)は3次元ＣＴの健側から患側の鏡像イメージを作成しこれを重ね合わせることで変形量を計測し術前計画を行った。しかし、両側の長管骨に変形を伴う場合はこの方法は行えない。

目的：ＣＴを用いた3次元的アライメント定量評価法を開発する。

方法：撮影したＣＴ dicomデータより骨領域を抽出し、3次元ＳＴＬモデルを作成。開発した専用ソフトウェアを用い、プログラムの中の特徴点を算出する機能を作り、画面上にてクリックする。①骨頭中心②大転子③小転子④内顆⑤外顆の５点を候補特徴点とし、これらを結ぶ線分の成す角で最小のものを３次元角度とした。また、特徴点の算出、角度計測にはＭＰＲ機能を搭載し決定した。先ずは大

腿骨上で3次元のLateral proximal femoral angle(以下PFA)、Lateral distal femoral angle （以下DFA)と回旋角を算出した。回旋角はレントゲンでの評価は困難であるが、3次元CT上では容易である。

症例:31歳男性。右大腿骨骨折後変形治癒にて当院紹介受診。3次元的変形量はPFA、DFA、回旋角の健側角/患側角はそれぞれ102.30°/78.88°，83.40°/90.50°，16.16°/51.06° であった。

今後: 今後症例を増やし有用性をさらに検討する。

31

Universal-Bar-Link創外固定器を用いた変形矯正における固定器設置位置・角度の誤差許容範囲の検討

Evaluation of mounting error tolerance for spatial position and posture in the deformity correction using the Universal-Bar-Link external fixator

○大橋 暁[1]、大西五三男[1]、池澤 賢治[2]、佐久間一郎[2]、松本 卓也[1]、中村 耕三[1]

[1] 東京大学整形外科、[2] 東京大学工学部新領域創成科学研究科

【背景】我々は、骨延長・変形矯正のための新規の片持ち式創外固定器であるUniversal-Bar-Link創外固定器(以下UBL)を開発し、本学会にて報告した。この創外固定器は、リンク機構結合部の回転軸を調節することで骨が仮想球中心を中心とした球運動を行うことで角度矯正を、また、カーボンシャフトに沿って移動することで骨延長を実現するものである。そのため、変形骨の変形中心と仮想球中心位置が一致すること(以下Position)、Mechanical Axisに対してカーボンシャフトを平行に配置すること(以下Posture)、以上の2点についてUBL創外固定器を設置する際に正確に行うことが重要である。本研究ではUBL創外固定器のPositionとPostureの許容される設置誤差を本創外固定器専用に開発したナビゲーションソフトにてシミュレーションし検討した。【方法】正常骨モデルおよび大腿骨重度変形モデルをモデル骨にて作製し、CT画像を基にそれぞれの表面形状モデルを作成した。変形骨モデルに対してCORAを算出し、理想的にUBL創外固定器を取付けた状態で正常骨を参照しながら整復シミュレーションを行い(以下NL)、整復後のmechanical lateral distal femoral angle(以下mLDFA)、lateral proximal femoral angle(以下LPFA)を測定した。また、UBL設置のPositionを三次元空間上6方向にそれぞれ5mmずつ偏位させた整復シミュレーション(以下Position)、UBL設置のPostureを正面像・側面像において5°傾けた整復シミュレーション(以下Posture)をNLと同様に行い、mLDFA、LPFAを測定しNLの測定値との差をそれぞれ算出した。【結果】PositionとNLの差の絶対値(平均±標準偏差)は、mLDFA：0.18±0.12°(最小0.05°、最大0.35°)、LPFA：0.18±0.13°(最小0.06°、最大0.36°)であった。また、PostureとNLの差の絶対値は、mLDFA：1.46±0.67°(最小0.69°、最大1.93°)、LPFA：0.51±0.08°(最小0.46°、最大0.60°)であった。【考察】Paleyらの報告ではmLDFA、LPFAは正常値が共に85°～90°であり、±約2°の残存角度は許容されると考えられる。今回の結果から、UBLの目標からの設置位置・角度誤差はそれぞれ5mm・5°以内であれば臨床的に許容範囲内であると考えられた。この許容範囲は手術において比較的容易に達成できるものであり、UBL創外固定器は臨床的に十分有用であると考えられる。

ELSEVIER

Ultrasound in Med. & Biol., Vol. 34, No. x, pp. xxx, 2008

0301-5629/08/$–see front matter

doi:10.1016/j.ultrasmedbio.2007.11.005

● *Original Contribution*

A NEW METHOD FOR EVALUATION OF FRACTURE HEALING BY ECHO TRACKING

JUNTARO MATSUYAMA,* ISAO OHNISHI,* RYOICHI SAKAI,† MASAHIKO BESSHO,* TAKUYA MATSUMOTO,* KOICHI MIYASAKA,† AKIMITSU HARADA,† SATORU OHASHI,* AND KOZO NAKAMURA*

*Department of Orthopaedic Surgery, University of Tokyo and †Research Laboratory, Aloka Co. Ltd., Tokyo, Japan

Abstract—Assessment of bone healing on radiographs depends on the volume and radio-opacity of callus at the healing site, but is not necessarily objective, and there are differences of judgment among observers. To overcome this disadvantage, a clinical system was developed to quantify the stiffness of healing fractures of the tibia in patients by the echo tracking (ET) method in a manner similar to a three-point bending test. The purpose of this study was to ensure that the ET system could clinically assess the progress, delay or arrest of healing. The fibular head and the lateral malleolus were supported. A 7.5-MHz ultrasound probe was placed on the proximal and distal fragments and a load of 25 N was applied. Five tracking points were set along the long axis of the ultrasound probe at intervals of 10 mm. With a multiple ET system, two probes measured the displacement of five tracking points on each of the proximal and distal fragments of the tibia, thereby detecting the bending of the two fragments generated by the load. ET angle was defined as the sum of the inclinations of the proximal and distal fragments. Eight tibial fractures in seven patients treated by a cast or internal fixation were measured over time. In patients with radiographically normal healing, the bending angle decreased exponentially over time. However, in patients with nonunion, the angle remained the same over time. It was demonstrated that the ET method could be clinically applicable to evaluate fracture healing as a versatile, quantitative and noninvasive technique. (E-mail: ohnishii-dis@h.u-tokyo.ac.jp) © **2008 World Federation for Ultrasound in Medicine & Biology.**

Key Words: **Ultrasound, Echo tracking, Fracture site stiffness, Fracture healing.**

INTRODUCTION

The most important issue in assessment of fracture healing is to obtain information about restoration of the mechanical integrity of the bone. In clinical practice, fracture healing is usually judged from serial radiographs. Assessment of bone healing on radiographs depends on the volume and radio-opacity of callus at the healing site, but is not necessarily objective, and there are differences of judgment among observers. In addition, radiographs cannot evaluate fracture site strength. In these respects, assessment of fracture healing by using radiographs is far from ideal.

The stated disadvantages of radiography for assessment of fracture healing have been pointed out in recent years, and various other methods of assessment have been developed. Jernberger (1970) devised an invasive method for measuring the bending stiffness of healing fractures of the tibia. With his method, the proximal and distal bone fragments were fixed by screws that were connected to a specially designed beam, and a load was applied through a screw at the center of the fixing screws. The method was based on the principle governing the bending of two beams connected at the ends and subjected to a bending force applied at the midpoint. Burny et al. (1984) developed a method that used a strain gauge attached to a fixator shaft. With their method, the strain gauge readings were monitored over time during weight bearing, and the pattern of fracture healing was classified into seven categories (such as normal, delayed, arrested, *etc.*). Assessment using acoustic emission (AE) was developed by Nicholls and Berg (1981), who detected acoustic pulses generated by microscopic failure of the bone under loading. The investigation by Watanabe et al. (2001) revealed that AE signals occurred with the yielding of callus. However, the strain gauge method and the AE method have the disadvantage that both are limited to patients with external fixation, and both require the in-

Address correspondence to: Isao Ohnishi, M.D., Ph.D., Department of Orthopaedic Surgery, University of Tokyo, 7–3–1 Hongo, Bunkyo-ku Tokyo, 113–0033, Tokyo, Japan.
E-mail: ohnishii-dis@h.u-tokyo.ac.jp

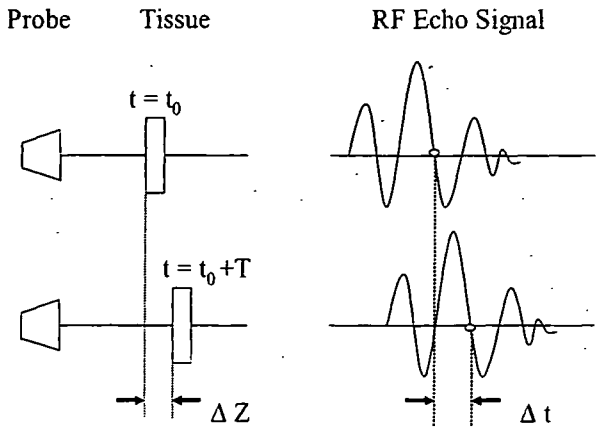

Fig. 1. The target tissue may move closer to or away from an ultrasonic probe over the distance ΔZ during a pulse repetition time of ultrasonic waves (T), causing phase delay of the RF echo signal (Δt). The ET method measures the extent of this displacement by tracking the initialized phase pattern of the echo signal.

sertion of screw pins or wires. For these reasons, such methods have not been widely used and a new method is needed that is both noninvasive and widely applicable.

To overcome such limitations, we developed a new method for the noninvasive and quantitative assessment of fracture healing. Bone always undergoes deformation in response to an applied load. By quantitatively measuring this deformation, it is possible to assess the mechanical properties of bone and thereby estimate the strength of a fracture site. In this study, we attempted to noninvasively assess the bending stiffness of the healing fracture sites after applying a load. To measure bending stiffness, we focused on ultrasound because it is noninvasive. Precise measurement of the displacement of a specific point can be done by the echo tracking (ET) method. This method is a technique for measuring minute displacement of a certain point on a tissue by detecting a wave pattern in the radiofrequency (RF) echo signal reflected from the target tissue (Fig. 1) (Hokanson et al. 1972). To apply this technique for detection of bone deformation, we improved it so that displacement could be measured with an accuracy of 2.6 μm (Matsuyama et al. 2006). We also developed a multi-ET system that was able to simultaneously track dynamic movement at multiple points on the bone surface. In our previous study of the three-point bending test using a porcine tibia, the strain gauge readings and the data from the multi-ET system showed an almost perfect linear correlation with the load ($r = 0.998$). These results indicated the possibility of using the echo tracking method to detect bone surface deformation.

The purpose of this study was to determine whether our newly developed ET system could clinically assess the progress, delay or arrest of healing by detecting the bending stiffness at the fracture healing site. Fracture healing was evaluated in patients with tibia fracture treated by a cast or internal fixation.

METHODS

A clinical system was developed to quantify the stiffness of healing fractures of the tibia in patients by the ET method in a similar manner to a three-point bending test. Five tracking points were set along the long axis of the ultrasound probe at intervals of 10 mm. With a multiple ET system, two probes measured the displacement of five tracking points on each of the proximal and distal fragments of the tibia, thereby detecting the bending of the two fragments generated by the load. ET angle was defined as the sum of the inclinations of the proximal and distal fragments (Fig. 2). When callus was weak in the initial stage of healing, the tracked points were almost in a straight line and the inclination of the two fragments was calculated directly. However, when the callus was more rigid in the late stage of healing, the line connecting the points was curved and the inclination was obtained from the slope of the linear regression equation for the displacement of the points.

Before clinical application of this method, its accuracy was evaluated by measuring the inclination of the metal flat panel.

Measurement of the accuracy of ET angle using an inclined flat metal panel

A flat stainless steel (SUS 420J) panel (length 270 mm, width 60 mm, thickness 5 mm) was used, which had a parallel accuracy and flatness variation of <2 μm. One end of the panel was attached to a magnet stand (DG, Noga Japan Ltd, Saitama, Japan), and the other side was attached to a goniometer (X13-001, Tsukumo Co. Ltd, Saitama, Japan) fixed to another magnet stand. Then, the

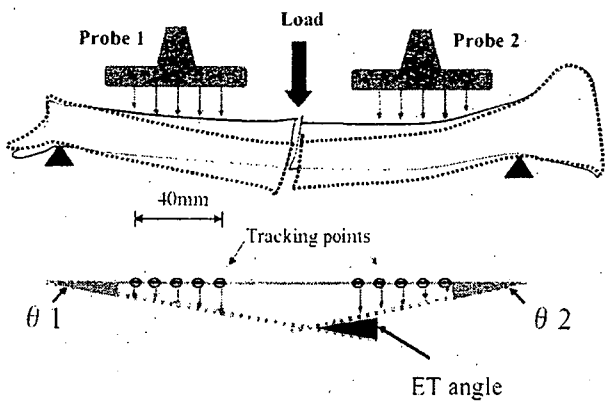

Fig. 2. Probes are set on each of the proximal and distal fragments of the tibia to detect the bending of the two fragments generated by a load. The ET angle is defined as the sum of the inclination of both fragments.

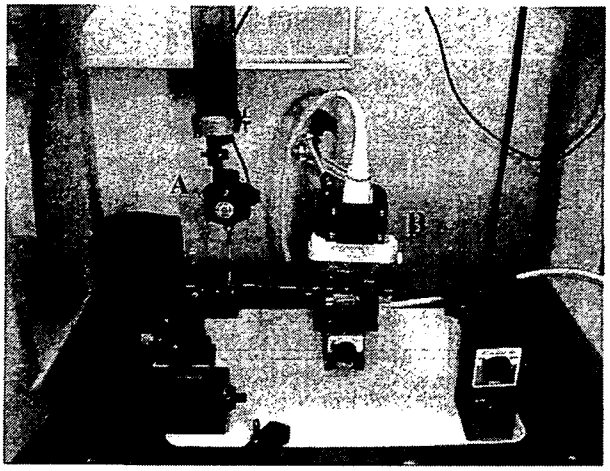

Fig. 3. The accuracy of the ET measurement was evaluated by measuring the inclination of the flat metal panel simultaneously using a 3-D measuring device. (A) 3-D measuring device; (B) 7.5-M Hz linear ultrasound probe.

metal panel was inclined by increasing the height of the goniometer stand. A 7.5-M Hz linear ultrasound probe (UST-5710-7.5, Aloka Co. Ltd., Tokyo) was set at a distance of 20 mm from the panel to measure the changes of displacement of each of five points on the panel (Fig. 3). Using these data, the ET angle of the panel was calculated. At the same time, the inclination of the panel was accurately measured using a 3-D measuring device (AE112, Mitsutoyo, Kanagawa, Japan) with an accuracy of 1 μm. The panel was inclined by elevating the sliding mechanism of the stand by 0.4 mm and the inclination of the panel was measured 5 times, after which the mean and standard deviation were calculated. Accuracy was evaluated by calculating the standard deviation of the difference between the ET angle and the inclination measured by the 3-D measuring device in each of the measurement trials.

Clinical measurement of fracture site bending stiffness

Eight tibial fractures in seven patients with an average age of 37 y (range 24–69 y) were measured (Table 1). Two fractures of two patients were treated conservatively with a cast, and six fractures of five patients were treated by internal fixation (locked intramedullary nailing in 4, plating in 1 and screws in 1). The average measurement period was 40.8 wk (21–60 wk), and the average number of measurements was 7.5 (5–11).

Patients assumed the supine position with both knees extended, and the affected leg was held horizontal with the antero-medial aspect of the tibia upwards. The fibular head and the lateral malleolus were supported and held tight by a Vacufix (Muranaka Medical Instrument Co., Ltd., Osaka, Japan) to avoid rotation of the leg during loading trials. Before measurement, B-mode images of the short axis of the proximal and distal fragments of the tibia were obtained to identify the center in both directions. By connecting both of the centers, the anatomical axis of the tibia was identified. A 7.5-MHz ultrasound probe was placed on the antero-medial aspect of each of the proximal and distal fragments in the long axis. Each probe was equipped with a multi-ET system with five tracking points at 10-mm intervals. The probes were set vertically on the skin of the leg and held tight with an articulated holder (DG61003, Noga Japan Ltd., Saitama, Japan). A load of 25 N was applied at a rate of 5 N/s and then reduced to 0 N at the same rate using a force gauge (DNP, Imada, Osaka, Japan) parallel to the direction of the probe at the most distal part of the proximal fragment adjacent to the fracture site (Fig. 4). For the initial measurement obtained in each patient, the loading point was set right on the long axis near the fracture site using a B-mode image as a guide. With this setup, the tibia was bent in the same way as for a three-point bending test in the direction of the ultrasound beam. In patients with oblique or spiral fractures, the loading point and the tracking points were set so that they did not cover the fracture site. In patients with a bone graft at the fracture site, the loading point was set on the graft, but the probes were placed so as not to cover it. In the patient with a plate, both the proximal and distal probes were set on the plate surface to measure bending of the plate. Using the multi-ET system, the probes

Table 1. Clinical cases of the tibial fracture

Case	Gender	Age	Limb	Treatment fracture healing	Measurement period (Initial-final)	Radiographic finding
1	F	24	L	Casting	4–47 wk	Normal
2	M	29	R	Casting	7–28 wk	Normal
3	M	23	R	Bone grafting	8–27 mo	Normal
4	M	31	R	Nailing	4–39 wk	Normal
5	F	57	R	Nailing	5–10 mo	Normal
6	F	57	L	Nailing	6–10 mo	Normal
7	F	26	R	Nailing	5 y 2 mo–5 y 7 mo	Nonunion
8	M	69	R	Plating	9–45 wk	Delayed

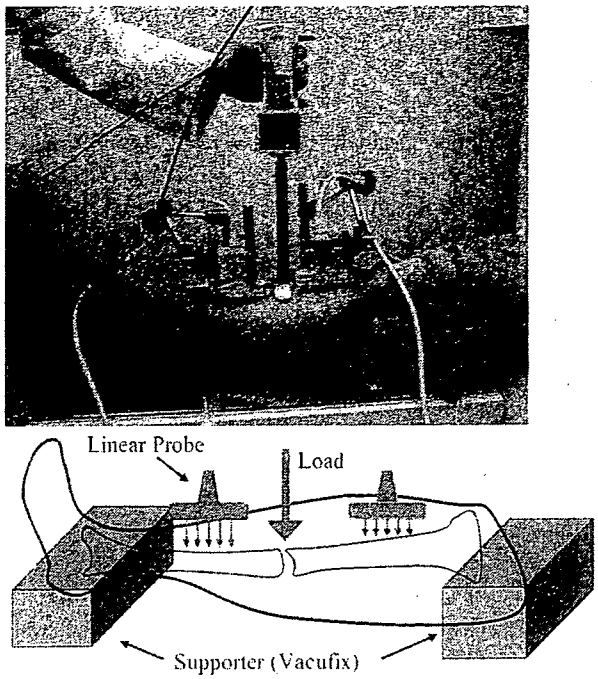

Fig. 4. The affected leg of a patient was held horizontal with the antero-medial aspect of the tibia upwards. The fibular head and the lateral malleolus were supported and held tight by a Vacufix. The probes were set vertically on the skin of the leg and held tight with an articulated arm. A load was applied using a force gauge parallel to the direction of the probe.

detected the angle between the proximal and distal fragments generated by the load. Measurement was repeated five times, and the mean and the standard deviation of the ET angle were calculated.

Fracture healing was assessed at intervals of two or three weeks until radiographic union or arrest of healing occurred. In each patient, the decrease of the ET angle was statistically examined to determine whether it decreased exponentially and whether the decrease was significant. To evaluate the changes of the ET angle over time, exponential regression analysis was performed, and the curve of the ET angle *vs.* time relation was drawn. Differences were considered significant when the p value was less than 0.05.

To investigate the influence of the position of the probes and the patient on the results, the precision of the method was evaluated by repeated measurement of the ET angle in a patient with a diaphyseal fracture of the tibia treated by a cast (case 2). In addition, the linearity of the relation between the load and the ET angle was assessed by incrementally increasing the load from 10 to 30 N. The ultrasound device (SSD 1000, Aloka Co. Ltd.) used in this investigation is used clinically and its safety has been established. The protocol of this investigation was approved by the ethics committee of The University of Tokyo Hospital, and the patients were enrolled after informed consent was obtained.

RESULTS

Accuracy of ET angle measurement for a flat metal panel

Measurement of the inclination of the flat metal panel showed that the average inclination was 0.117° and the standard deviation was 0.002°. The average inclination obtained with the 3-D measuring device was 0.116°, with a standard deviation of 0.003°. The standard deviation of the differences between the data obtained by the ET method and by the 3-D measuring device was 0.002°.

Clinical measurement of fracture site bending stiffness

The average time required for measurement was 17 min (range 15–20 min). At each loading trial, none of the patients complained of pain and there were no complications related to measurement.

The precision of this method was evaluated by repeating measurement of case 2 (treated with a cast), with repositioning of the leg and the ultrasound probes. The mean and standard deviation of the ET angle were 0.316 ± 0.015, and the coefficient of variation was calculated to be 4.6%. The linearity of the relation between the load and the bending angle was very high, with a correlation coefficient of 0.997.

Cases presentation

Case 1: A 24-year-old-woman treated with a cast. The patient sustained a spiral fracture of the proximal diaphysis of the tibia in a traffic accident, and a patella tendon bearing brace cast was applied. Healing was assessed by the ET method, as well as radiographs a total of 11 times from 4 weeks to 47 weeks after fracture. The fracture line became opaque and the callus volume increased from 4 weeks to 19 weeks, but after 26 weeks there was almost no change of the thickness of the callus. On the other hand, measurement showed that the ET angle was about 1° at 4 weeks, and that it decreased exponentially ($y = 1.40e^{-0.105x}$, $r = -0.975$, $p < 0.0001$). The ET angles of both cases 1 and 2 treated with a cast decreased exponentially over time and they reached the level of the intact side by 22 weeks (Fig. 5a, b).

Case 7: A 26-year-old-woman with a fracture of the diaphysis of the tibia treated by a locked intramedullary nailing. ET measurement was performed five times from 5 y 2 mo to 6 y 7 mo after fracture. Her X-ray films showed hypertrophic nonunion, but judgment whether healing was proceeding was extremely difficult. ET measurement showed that there was no significant decrease of the angle over a period of 1 y and 5 mo ($y = 0.264e^{0.002x}$, $r = 0.238$, $p = 0.700$) (Fig. 6a, b).

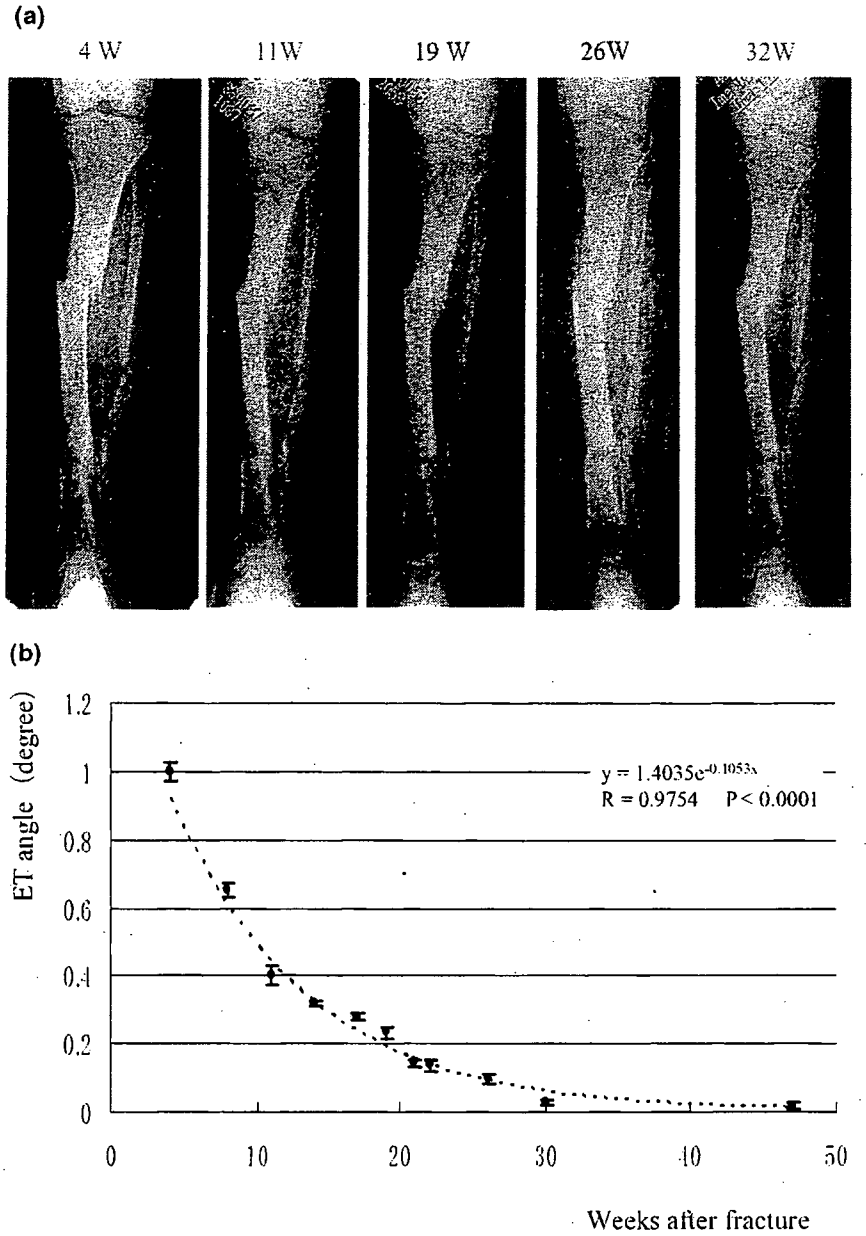

Fig. 5. (a) Time sequential change of the fracture site X-ray from 4 weeks to 32 weeks after fracture in case 1 treated with casting. The fracture site healed normally. (b) In the same patient, the ET angle was plotted. The ET angles decreased exponentially over time.

Case 8: A 69-year-old-man with a long oblique fracture treated with a plate. His X-ray films showed a long oblique fracture line extending for almost 80 mm. Measurement was performed 10 times from 9 weeks to 45 weeks after fracture, during which period almost no change of the fracture site or callus was recognized on X-ray films. The ET method measured the bending angle of the plate. The change was very slow, but the angle decreased significantly from 0.28 to 0.2 degrees, and then finally declined to 0.1 degree. The overall change showed an exponential curve ($y = 0.40e^{-\cdots t}$, $r = -0.895$, $p = 0.0005$) (Fig. 7a, b). In patients with radiographically normal healing, the bending angle decreased exponentially over time (Fig. 8). However, in patients with nonunion, the angle remained the same over time.

DISCUSSION

Our method allows noninvasive assessment of bending stiffness at the healing site, so it can be appli-

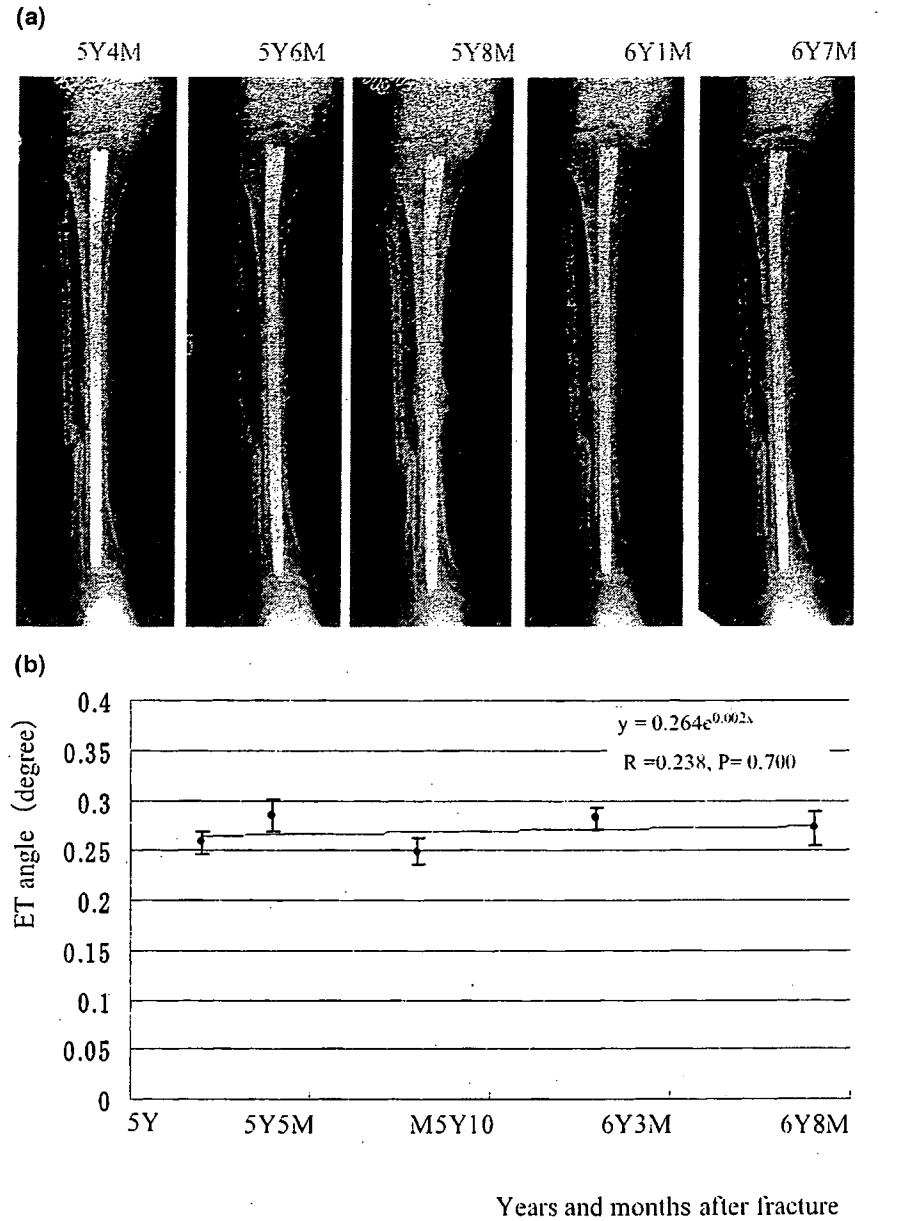

Fig. 6. (a) Time sequential change of the fracture site X-ray from 5 y 4 mo to 6 y 7 mo after fracture in case 7, treated with intramedullary nailing. The X-ray films showed hypertrophic nonunion, but judgment of whether healing was proceeding was extremely difficult. (b) In case 7, the ET angle showed no change over time and the regression lines showed no significant decrease.

cable to patients treated conservatively as well as those managed by surgical intervention with plating or intramedullary nailing.

In this study, the precision and reproducibility of the method were evaluated. The precision of measuring displacement by using the echo tracking system specially designed for bone surface measurement has already been assessed, and a precision of 2.6 μ was demonstrated in our previous study. However, the precision of measuring the bending angle has not been investigated before. We obtained a precision of 0.002°, which was thought to be adequate based on the results of the study by Moorcroft et al. (2001) that evaluated fracture healing. They used the three-point bending test to generate angles of 0.4 to 1.0° in an *in-vivo* measurement trial and connected a goniometer to the bone fragment *via* screw pins fixed to a side bar of the external fixator to detect bending at the fracture site.

When estimation of the linearity of measurement was done in relation to the load, there was excellent

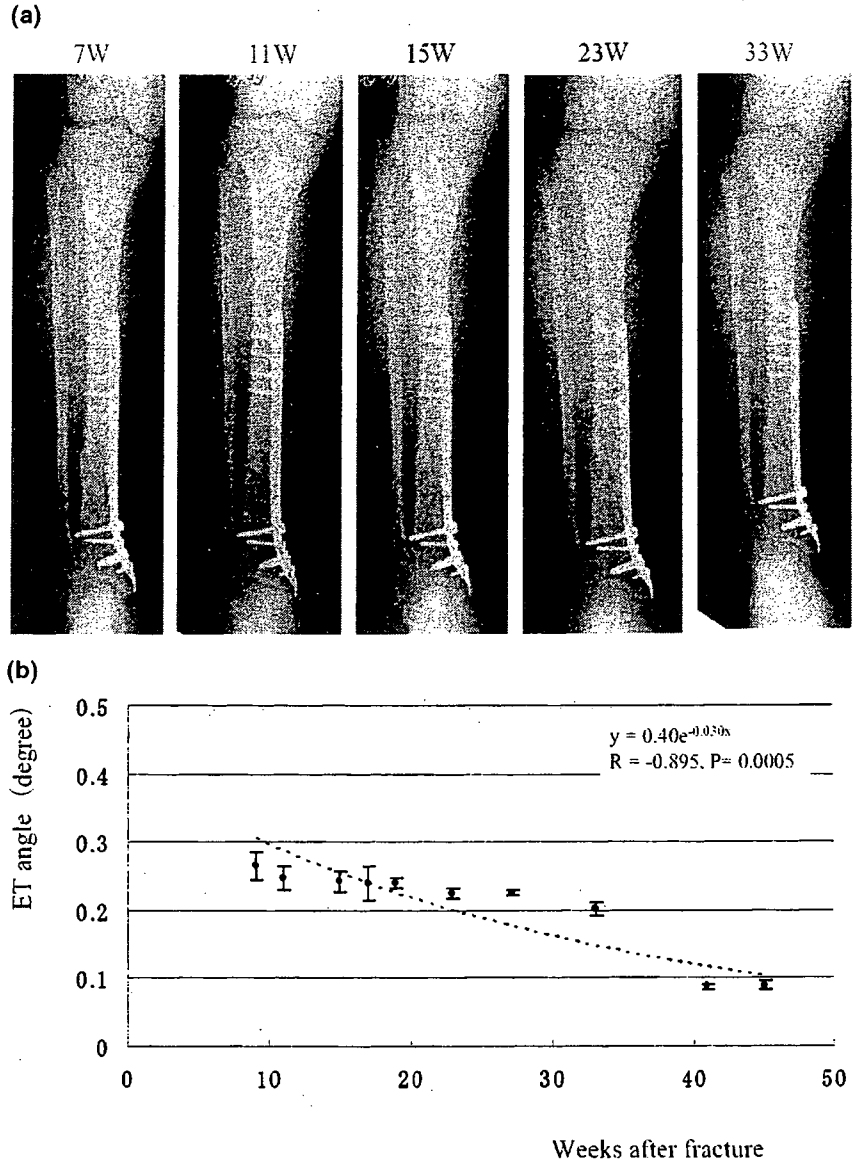

Fig. 7. (a) The X-ray films of case 8, treated with plating. No change of the fracture site or callus was recognized on X-ray films. (b) The ET method measured the bending angle of the plate. The change was very slow, but the angle decreased significantly from 0.28 to 0.2°, and then finally declined to 0.1°.

linearity between magnitude of the load and the ET angle ($r = 0.997$), indicating that elastic deformation of the fracture site had occurred under a load range of 10 to 30 N. Therefore, measurement was shown to be noninvasive as well as safe, without causing any residual deformity.

Reproducibility of the measurement method was estimated to be 0.015°, which was adequate to evaluate fracture healing quantitatively, because the angle ranged from around 1° in the initial stage to about 0.1° in the final stage when it was almost equivalent to that of the intact tibia. However, we have to improve the reproducibility of measurement *in vivo*. The factors affecting reproducibility *in vivo* include the position of the leg, loading direction and positions of the probes. Among these, the positioning or fixation of the leg seems to have the most influence on the reproducibility of measurement.

For clinical evaluation of fracture healing, data obtained by the ET method were compared with X-ray findings over time. In patients with delayed healing or nonunion, judgment of the healing process using X-ray films was difficult because the direction and conditions of obtaining images were not exactly the same every time, so the findings were not reproducible. In contrast, the echo tracking method evaluated fracture stiffness